# Spin-Orbit Twisted Spin Waves: Group Velocity Control

F. Perez,[1,*] F. Baboux,[1,2] C. A. Ullrich,[3] I. D'Amico,[4] G. Vignale,[3] G. Karczewski,[5] and T. Wojtowicz[5]

[1]*Institut des Nanosciences de Paris, CNRS/Université Paris VI, Paris 75005, France*
[2]*Laboratoire de Photonique et de Nanostructures, LPN/CNRS, 91460 Marcoussis, France*
[3]*Department of Physics and Astronomy, University of Missouri, Columbia, Missouri 65211, USA*
[4]*Department of Physics, University of York, York YO10 5DD, United Kingdom*
[5]*Institute of Physics, Polish Academy of Sciences, Al. Lotnikow 32/46, 02-668 Warsaw, Poland*

(Received 10 May 2016)

We present a theoretical and experimental study of the interplay between spin-orbit coupling (SOC), Coulomb interaction, and motion of conduction electrons in a magnetized two-dimensional electron gas. Via a transformation of the many-body Hamiltonian we introduce the concept of spin-orbit twisted spin waves, whose energy dispersions and damping rates are obtained by a simple wave-vector shift of the spin waves without SOC. These theoretical predictions are validated by Raman scattering measurements. With optical gating of the density, we vary the strength of the SOC to alter the group velocity of the spin wave. The findings presented here differ from that of spin systems subject to the Dzyaloshinskii-Moriya interaction. Our results pave the way for novel applications in spin-wave routing devices and for the realization of lenses for spin waves.

DOI:

Spin-wave based transistors are an appealing alternative to the traditional charge-based transistor, since spin waves carry information with reduced dissipation compared to charge currents [1,2]. However, one still has to develop efficient methods for controlling the spin waves with low energy cost, a condition not satisfied by the manipulation with magnetic fields. Spin-orbit coupling (SOC) for conduction electrons is a quantum-relativistic interaction emerging for spin-wave control [3–9]. An extensive body of literature has been devoted to spin waves in ferromagnets subject to the Dzyaloshinskii-Moriya interaction (DMI). The DMI arises from SOC [10,11] and causes chiral spin-wave dispersions [7,12] and damping [13]. In most systems the DMI energy $D$ remains an empirical parameter with a magnitude of a few percent of the exchange energy $J$ [3,14,15].

The DMI is perfectly suited for spins strongly or weakly localized. However, for delocalized spins in a Galilean invariant system, for which the kinetic energy interplays with the Coulomb exchange and the SOC, all three protagonists are responsible for the spin-wave dynamics, like in a magnetic two-dimensional electron gas (2DEG). One thus expects a new type of behavior for the spin waves. In our previous works [6,16], we used the concept of a macroscopic spin-orbit field enhanced by interactions. Here, by contrast, we predict the amplitude and direction of the chiral wave-vector shift of spin waves using a transformation of the many-body Hamiltonian of a magnetic 2DEG. We introduce the concept of spin-orbit twisted spin waves and report conclusive experimental evidence. This leads us to the possibility of optically tuning the electron density to modify and even reverse the group velocity of the spin waves. We observe significant differences between the spin-orbit twisted spin waves and the DMI spin waves. Thus, in delocalized spin systems, our findings show that SOC offers the opportunity to control both the direction and velocity of spin waves without affecting the spin-wave stiffness and the damping rate.

*Spin waves in a magnetic 2DEG.*—We focus on spin-wave excitations of a magnetic 2DEG embedded in a doped $Cd_{1-x}Mn_xTe$ quantum well containing a fraction $x = 0.013$ of substitutional Mn impurities. This system is ideal to study spin excitations of itinerant two-dimensional electrons, because of its simple free-electronlike conduction band. The application of a moderate magnetic field $\mathbf{B}$ (of order 2 T) parallel to the plane of the quantum well polarizes the spins localized on the randomly distributed Mn atoms, which in turn polarizes the electron gas through exchange interaction [17]. This causes a Zeeman splitting $Z$ of order meV of the electronic states in the conduction band [18], with a negligible orbital quantization. One thus obtains a spin-polarized 2DEG, with two spin-split parabolic sub-bands. The 2DEG electron density (the number of electrons per unit area) is $n_{2D} = 2.7 \times 10^{11}$ cm$^{-2}$ and the mobility is $1.7 \times 10^5$ cm$^2$/V s.

Such a 2DEG supports spin-wave modes located in the energy gap below the continuum of single-particle excitations, the paramagnet equivalent of the Stoner continuum [29–31]. The energy dispersion of these spin waves is quadratic with the in-plane momentum $\mathbf{q}$ [31–33],

$$\hbar\omega_{\mathrm{sw}}(\mathbf{q}) = Z + S_{\mathrm{sw}}\frac{\hbar^2}{2m^*}q^2 + i\eta_q. \tag{1}$$

Here, $\omega_{\mathrm{sw}}(\mathbf{q})$ is the spin-wave angular frequency, $S_{\mathrm{sw}}$ is the spin-wave stiffness in units of $\hbar^2/2m^*$, $m^*$ is the electron band mass [34], and $\eta_q = \eta_0 + \eta_2 q^2$ is a momentum-dependent

damping rate, also quadratic in $q$, which has an intrinsic part ($\eta_2 q^2$) caused by a friction with multiple single-particle excitations [35,36] as experimentally shown [32] and a sample dependent part ($\eta_0$) dominated by magnetic disorder [32]. In contrast with magnons in ferromagnets, $S_{sw}$ is here a negative number; i.e., the spin-wave energy starts at the bare Zeeman energy $Z$ and then decreases, until it merges with the single-particle continuum where Landau damping occurs.

*Spin-orbit twisted spin waves.*—A 2DEG electron occupying the quantum state $|\mathbf{k}\rangle$ is subject to a $\mathbf{k}$-dependent spin-orbit magnetic field $\mathbf{B}_{so}(\mathbf{k})$ [see Fig. 1(b)]. Hence, one might expect that the spin-wave dynamics (stiffness and damping) should be affected by the set of individual SO fields. However, we show that the collective behavior is influenced in a rather simple way as a consequence of symmetries embedded in the SOC.

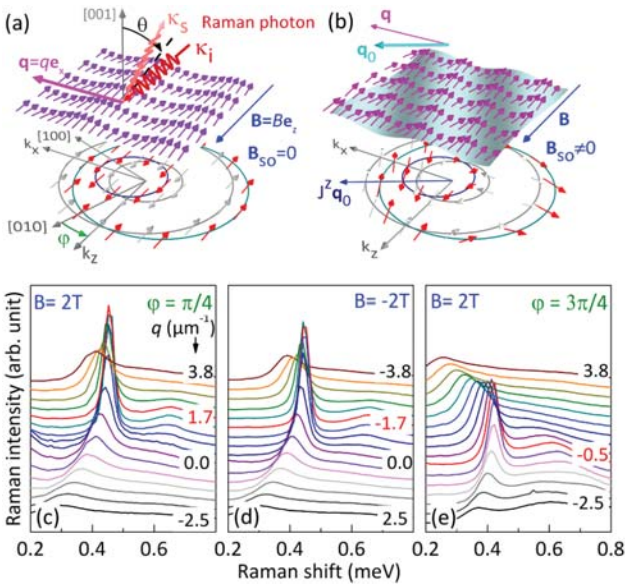


FIG. 1. (a) Top plane: Raman incoming ($\boldsymbol{\kappa}_i$) and outgoing ($\boldsymbol{\kappa}_s$) photon wave vectors. $\mathbf{q}$ is the in-plane momentum of the spin wave probed by the Raman process. The amplitude and direction of $\mathbf{q}$ are controlled by $\theta$ and $\varphi$, respectively. The magnetic field, parallel to $\mathbf{e}_z$, is always perpendicular to $\mathbf{q}$. Bottom plane: the spin-wave oscillation in real space is associated with an out-of-phase oscillation of the two Fermi disks in momentum space with respect to their equilibrium positions (gray circles). Electron spins remain parallel or antiparallel to $\mathbf{B}$. (b) Illustration of the spin-wave twisting caused by SOC. Bottom plane: the momentum-space motion twists the spins with respect to their equilibrium positions (gray vectors). A $z$-spin current parallel to $\mathbf{q}_0$ appears. Top plane: the spins now evolve in a moving wavelike reference frame (highlighted by the blue shading). Consequently, the spin waves are twisted with a phase $\mathbf{q}_0 \cdot \mathbf{r}$ (see text). [(c)–(e)] Electronic Raman spectra obtained by varying the momentum $\mathbf{q}$ for [(c) and (d)] $\varphi = \pi/4$, $B = \pm 2$ T, and (e) $\varphi = 3\pi/4$, $B = 2$ T. The low-energy Raman line, sharply peaked, is a signature of the spin wave. The smoother structure at higher energy is due to single-particle excitations. The spectrum highlighted in red for each case shows the spin-wave maximum energy.

The Hamiltonian of our 2DEG has two parts: $\hat{H} = \hat{H}_0 + \hat{H}_{SO}$. $\hat{H}_0$ describes a translationally invariant interacting 2DEG subject to a constant magnetic field applied in the plane of the quantum well and without Landau orbital quantization [18,31]. The Coulomb interaction in $\hat{H}_0$ leads to the formation of spin waves [31], which propagate with the dispersion of Eq. (1). $\hat{H}_{SO}$ is the Hamiltonian due to SOC in the conduction band: $\hat{H}_{SO} = \sum_i \mathbf{B}_{so}(\mathbf{k}_i) \cdot \hat{\boldsymbol{\sigma}}_i$ couples the in-plane component of the $i$th electronic spin $\hat{\boldsymbol{\sigma}}_i$ with its momentum $\mathbf{k}_i$.

SOC arises from two broken inversion symmetries of the quantum well [37]: the Rashba contribution [38], of strength $\alpha$, due to the asymmetric doping along the growth direction [001], and the Dresselhaus contribution [39], of strength $\beta$, due to the asymmetry of the CdTe crystalline unit cell. The Rashba part in $\mathbf{B}_{so}(\mathbf{k})$ lies in the 2DEG plane perpendicular to the electron momentum $\mathbf{k}$; the Dresselhaus part has mirror symmetry with respect to the crystalline axis [100]. The resulting SOC field is given by

$$\mathbf{B}_{so}(\mathbf{k}) = \alpha \mathbf{k} \times \mathbf{w} + \beta[(\mathbf{k} \cdot \mathbf{u})\mathbf{u} - (\mathbf{k} \cdot \mathbf{v})\mathbf{v}], \qquad (2)$$

where the unit vectors $\mathbf{u}$, $\mathbf{v}$, and $\mathbf{w}$ are along the crystallographic directions [100], [010], and [001].

When expressing $\hat{H}_{SO}$ in the in-plane coordinates $(x, z)$, where $\mathbf{B} = B\mathbf{e}_z$ and $\mathbf{q} = q\mathbf{e}_x$, as sketched in Fig. 1(a), we find, to linear order in $\mathbf{k}$, $\hat{H}_{SO} = -\hbar \mathbf{q}_0 \cdot \hat{\mathbf{J}}^z + \hbar \mathbf{q}_1 \cdot \hat{\mathbf{J}}^x$. Here, $\hat{\mathbf{J}}^\nu = (1/2m^*) \sum_i \hat{\mathbf{p}}_i \hat{\sigma}_{\nu,i}$ is the homogenous spin current of the $\nu$-spin component. The change of coordinates naturally introduces the two wave vectors $\mathbf{q}_0$ and $\mathbf{q}_1$, where

$$\mathbf{q}_{\{1\}}^{\{0\}} = (2m^*/\hbar^2)[(\alpha \pm \beta \sin 2\varphi)\mathbf{e}_{\{z\}}^{\{x\}} + \beta \cos 2\varphi \mathbf{e}_{\{x\}}^{\{z\}}]. \qquad (3)$$

Note, first, that the second term in $\hat{H}_{SO}$ couples to the transverse spin components and thus only produces energy corrections to second order in SOC [18]. We therefore neglect it as we limit ourselves to first order considerations. By contrast, the first term in $\hat{H}_{SO}$ couples to the longitudinal spin components $\hat{\sigma}_{z,i}$. Its effect can be similar to a magnetic field along $z$, but activated by the electron motion embedded in the spin-wave oscillation. We can thus infer that its strength is periodic in real space: the spin wave creates a $\mathbf{q}$ periodicity of the spin phases resulting in a $\mathbf{q}$ periodicity of $\hat{\mathbf{J}}^z$, which in turn twists the spins periodically in the direction of $\mathbf{q}_0$. A positive feedback occurs, leading to the simple addition of spatial phase changes $\mathbf{q} + \mathbf{q}_0$ in the spin-wave dispersions as depicted in Fig. 1(b).

We can rigorously demonstrate this "spin-orbit twist" effect by a gauge transformation of $\hat{H}$ with the twist operator $\hat{U} = e^{-i \sum_i \mathbf{q}_0 \cdot \mathbf{r}_i \hat{\sigma}_{z,i}/2}$ [40]. This transforms the momentum operator of the $i$th electron into

$\hat{U}\hat{\mathbf{p}}_i\hat{U}^\dagger = \hat{\mathbf{p}}_i + \hbar\mathbf{q}_0\hat{\sigma}_{z,i}/2$, and $\hat{H}$ becomes $\hat{U}\,\hat{H}\,\hat{U}^\dagger = \hat{H}_0$, where we neglected terms in the second order of the SOC [18]. Hence, the twist operator restores the spin-rotational invariance [41,42]. $\hat{U}$ imprints a spin rotation along $z$ with a spatially dependent angle that grows at a rate $q_0$ along the $\mathbf{q}_0$ direction. Consequently, the spin-wave operator is transformed into $\hat{U}\hat{S}_{+,\mathbf{q}}\hat{U}^\dagger = \hat{S}_{+,\mathbf{q}+\mathbf{q}_0}$.

The final result is that, to first order in SOC, the spin-wave operators are unchanged, apart from shifting the spin-wave momentum by $\mathbf{q}_0$. The spin-wave equation of motion in the presence of SOC reads

$$i\hbar\frac{d}{dt}\hat{S}_{+,\mathbf{q}} = [\hat{S}_{+,\mathbf{q}}, \hat{H}] = \hat{U}^\dagger[\hat{S}_{+,\mathbf{q}+\mathbf{q}_0}, \hat{H}_0]\hat{U}. \quad (4)$$

This equation leads to a spin-wave dispersion and damping shifted by a wave vector $-\mathbf{q}_0$, while protecting the spin-wave stiffness that remains unaffected by SOC,

$$\hbar\omega_{\mathrm{sw}}^{\mathrm{SO}}(\mathbf{q}) = Z + S_{\mathrm{sw}}\frac{\hbar^2}{2m^*}|\mathbf{q}+\mathbf{q}_0|^2 + i\eta_{\mathbf{q}+\mathbf{q}_0}. \quad (5)$$

Equations (4) and (5) can be interpreted as follows: the gauge transformation performed above is equivalent to a quantum change of reference frame in the spin space, the latter depending on instantaneous positions of electrons. The new reference frame for the spins is then moving, following the electron oscillation in real space [see Fig. 1(b)]. In this new spin frame, the spin wave experiences a constant and uniform magnetic field: its propagation is determined by $\hat{H}_0$ only. This effect is similar to the drag of optical or acoustic waves in a moving medium [43,44], except that here the moving medium refers to the spin space.

*Spin-orbit twist effect evidenced by Raman spectra.*—To measure the spin-wave dispersions of Eq. (5) we employ electronic Raman scattering, which transfers a well-controlled momentum $\mathbf{q} = \boldsymbol{\kappa}_{i,\parallel} - \boldsymbol{\kappa}_{s,\parallel} \simeq 2\kappa_i \sin\theta\mathbf{e}_x$ to the spin excitations, where $\boldsymbol{\kappa}_i$ and $\boldsymbol{\kappa}_s$ are the momenta of the linearly cross-polarized incoming and scattered photons, respectively. The experimental geometry shown in Fig. 1(a) defines the incidence angle $\theta$ and the in-plane azimuthal angle $\varphi$, which control the magnitude and direction of $\mathbf{q}$, respectively. The in-plane orientation of the magnetic field $\mathbf{B} = B\mathbf{e}_z$ is adjusted so that it is always perpendicular to $\mathbf{q} = q\mathbf{e}_x$. $\mathbf{q}$ and $\mathbf{B}$ are at the angle $\varphi$ with, respectively, the [100] and [010] crystalline directions. The accurate $\varphi$ control of $\mathbf{q}$ is crucial to evidence the SOC effects on spin waves.

Figures 1(c)–1(e) show a series of electronic Raman spectra, obtained at fixed $\varphi = \pi/4$ and $B = \pm 2$ T, and for transferred momenta $q$ between $\mp$ 2.5 and $\pm 3.8$ $\mu\mathrm{m}^{-1}$ [the positive sign is defined by the orientation of $\mathbf{q}$ in Fig. 1(a)]. The most prominent feature in both series of spectra is the strong spin-wave Raman line. However, in contrast with the spin-wave dispersion relation (1), which is valid without SOC, we observe that for $\varphi = \pi/4$ and $B = +2$ T, the highest spin-wave energy and the minimum linewidth are not at $q = 0$, but shifted to $q = q_s \simeq 1.7$ $\mu\mathrm{m}^{-1}$ (see the red spectrum). When inverting $B$ to $-2$ T, the series looks very similar after inversion of the momentum axis. The extrema occur symmetrically, at $q_s \simeq -1.7$ $\mu\mathrm{m}^{-1}$.

These observations are illustrated in Figs. 2(a) and 2(b), which present the energy and linewidth dispersions as a function of $q$, at $\varphi = \pi/4$, for both directions of the magnetic field. Since the linewidth $\eta$ of the spin-wave Raman line yields the damping rate $\eta_q$ of Eq. (1), Figs. 2(a) and 2(b) demonstrate that the SOC lifts the chiral degeneracy of the spin-wave energy as well as of the damping rate: the spin-wave energy and linewidth dispersions are both asymmetric and invariant under simultaneous inversion of the directions of the magnetic field and the wave vector.

Figure 1(e) shows a series of electronic Raman spectra obtained at $B = +2$ T, but for a different azimuthal angle $\varphi = 3\pi/4$. The momentum shift now changes to

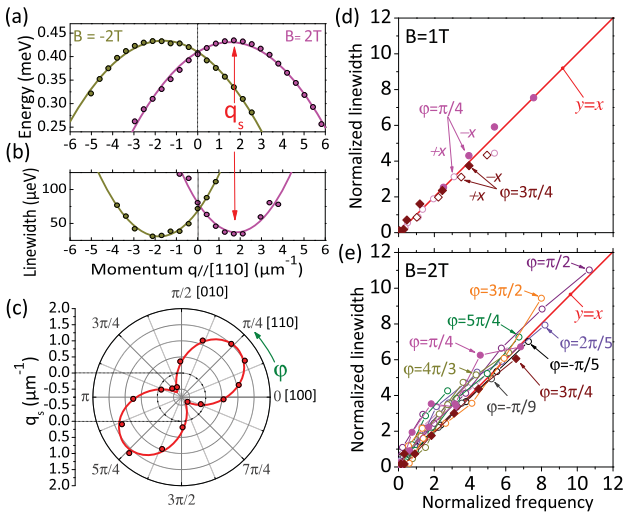


FIG. 2. [(a) and (b)] Lifting of the spin-wave chiral degeneracy by a momentum shift of the dispersions due to SOC: Momentum dispersion of energy (a) and linewidth (b) of the spin wave for $\varphi = \pi/4$ and $B = \pm 2$ T. Dispersions are shifted by $q_s$ from $q = 0$ with a mirror symmetry when inverting the magnetic field. (c) (circle) represents the $q_s$ dependence with $\varphi$, which has been extracted from the dispersions measured for $\varphi \in [(-\pi/4), (3\pi/2)]$. The red curve is a fit of $q_s(\varphi)$ to the $x$ component of $-\mathbf{q}_0$ given by Eq. (3). [(d) and (e)] Universal linear relation between the linewidth and the energy of the spin wave: $(\eta - \eta_0)/\eta_2$ is plotted as a function of $\frac{2m^*}{\hbar^2}(\hbar\omega - Z)/S_{\mathrm{sw}}$; symbols of the same color are for a given in-plane angle $\varphi$, but for various values of $q$. (d) $B = +1$ T; open (solid) symbols correspond to spin waves with wave vector $\mathbf{q}$ directed towards $-\mathbf{e}_x$ ($+\mathbf{e}_x$). (e) $B = +2$ T; solid symbols correspond, here, to the two extremal angles $\varphi = \pi/4$, $3\pi/4$; open symbols are for other angles.

$q_s \simeq -0.5\ \mu\text{m}^{-1}$, which suggests a modulation of $\mathbf{q}_s$ with $\varphi$. Indeed, Fig. 2(c) represents the experimental $q_s$ extracted from the dispersions measured for various in-plane angles $\varphi$. $q_s$ matches the $\mathbf{e}_x$ component of $-\mathbf{q}_0$. The $\pi$-periodicity of the $q_s(\varphi)$ modulation is in complete agreement with the $C_{2v}$ in-plane symmetry of the SOC arising from the superposition of the Rashba and Dresselhaus contributions and leading to the expression of $\mathbf{q}_0$ given in Eq. (3). Fitting the experimental values with Eq. (3) yields the Rashba and Dresselhaus constants $\alpha$ and $\beta$ with high accuracy: we find $\alpha = 1.83 \pm 0.08$ meV Å and $\beta = 3.79 \pm 0.11$ meV Å. To summarize, the quadratic energy and damping dispersions are both shifted by a $\mathbf{q}_s$ modulated with $\varphi$, while the spin-wave stiffness $S_{\text{sw}} \simeq -27.5 \pm 2.6$ and damping $\eta_2 \simeq 9.9 \pm 2.0$ eV $\mu\text{m}^2$ remain protected.

Chirality in spin-wave energy dispersions and chiral damping has been observed in Fe monolayers [7]. Chiral damping dispersions have been observed in Pt/Co/Ni films [13]. However, Eqs. (1) and (5) show a universal linear relation between the damping rate and angular frequency of the spin wave, independent of SOC, which reads

$$\eta = \tilde{\eta}_0 + \frac{2m^*}{\hbar}\frac{\eta_2}{S_{\text{sw}}}\omega, \tag{6}$$

where $\omega$ stands for either $\omega_{\text{sw}}$ or $\omega_{\text{sw}}^{\text{SO}}$, and $\tilde{\eta}_0 = \eta_0 - 2mZ/\hbar^2 S_{\text{sw}}$. This universal linear behavior is demonstrated in Figs. 2(d) and 2(e) where the linewidth has been plotted as a function of energy for $B = +1$ T and $B = +2$ T and various in-plane angles. The chirality and anisotropy do not appear anymore: $+\mathbf{e}_x$ and $-\mathbf{e}_x$ waves, for every $\varphi$, fall on the same line, which shows that the relation between spin-wave energy and damping does not depend on SOC but only on the Coulomb and kinetic interactions present in $\hat{H}_0$. This confirms the existence of spin-orbit twisted spin waves predicted in Eq. (5). Moreover, the linear relation of Figs. 2(d) and 2(e) was not found in Ref. [13]. This unambiguously establishes the new physics underlying the spin-orbit twisted spin waves.

*Spin-wave group velocity control.*—We can now focus on the group velocity vector given by $\mathbf{v}_g = \nabla_q \omega_{\text{sw}}$. In the absence of SOC, $\mathbf{v}_{g,\mathbf{q}} = S_{\text{sw}}\hbar\mathbf{q}/m^*$ is radial and vanishes at zero momentum. In the presence of SOC, Eq. (5) yields $\mathbf{v}_{g,\mathbf{q}} = S_{\text{sw}}\hbar(\mathbf{q} + \mathbf{q}_0)/m^*$. Except for $\varphi = \pi/4 (\text{mod}\, \pi/2)$, $\mathbf{v}_{g,\mathbf{q}}$ has acquired a nonradial component. The radial component vanishes along the $q = -q_{0x}$ curve. At $q = 0$, the group velocity is no longer 0 and depends on the respective directions of the magnetization and crystalline axis: $\mathbf{v}_{g,q=0} = S_{\text{sw}}\hbar\mathbf{q}_0/m^*$.

Since $\mathbf{q}_0$ depends on the magnetization direction and on the strength of the Rashba and Dresselhaus constants [Eq. (3)], the spin-orbit twist introduces a new way to control the spin-wave propagation direction, e.g., by varying the density by optical gating [18]. With this technique, the electron density can be reproducibly reduced by up to a factor of 2 in our sample. We set $B = 2$ T, and for each density we repeat the procedure exposed in Fig. 2 to extract the quantities $S_{\text{sw}}$, $\alpha$, and $\beta$ and evaluate the group velocity. Respective variations of the spin-wave stiffness, $\alpha$ and $\beta$, with the density are given in Supplemental Material [18].

The group velocity control is summarized in Fig. 3, for the specific case of $\varphi = 3\pi/4$. The momentum shift $\mathbf{q}_s$ (red dots) is plotted as it varies with the density $n_{2\text{D}}$. Standing spin waves correspond to the curve $q = q_s(n_{2\text{D}})$. When departing from this curve, the group velocity acquires a positive or negative component, which for that specific angle ($\varphi = 3\pi/4$) is always collinear with $\mathbf{q}$. For example, at fixed momentum transfer $q = -0.6\ \mu\text{m}^{-1}$, the spin wave propagates upward when $n_{2\text{D}} = 2.7 \times 10^{11}$ cm$^{-2}$ and downward for $n_{2\text{D}} = 1.5 \times 10^{11}$ cm$^{-2}$. This illustrates the control of the spin-wave propagation direction that can be obtained via density control by optical gating (as shown here) or by electrical gating.

In conclusion, we showed that the interplay of SOC and Coulomb interaction in itinerant electronic systems profoundly affects the spin-wave dynamics. Our first-principles predictions and related experimental confirmation demonstrate that, to leading order in the Rashba and Dresselhaus field strengths, the dispersions in energy and damping rate are both simply rigidly shifted by a wave vector $\mathbf{q}_0$ without any change of the universal relation between damping and energy. The rigid shift is similar to that of spin waves subject to Dzyaloshinskii-Moriya interaction (well suited for localized spins). However, the conservation of the universal relation is new. This

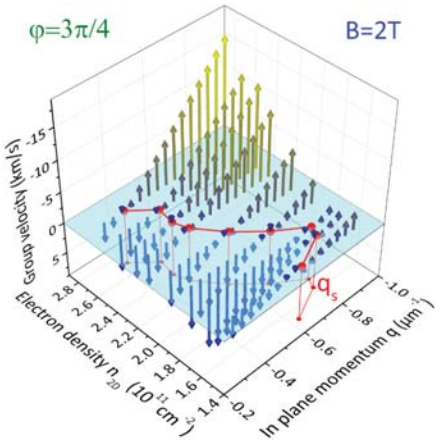


FIG. 3. Optical gating of the spin-wave group velocity. The group velocity vector changes for $\varphi = 3\pi/4$ and $B = 2$ T as a function of momentum and electron density (note that the group velocity is purely longitudinal at $\varphi = 3\pi/4$): a spin wave with momentum $q = -0.5\ \mu\text{m}^{-1}$ experiences an inversion of its group velocity when the density is changed from 1.8 to $2.7 \times 10^{11}$ cm$^{-2}$. The red dots, where $q = q_s$, indicate a standing spin wave.

leads us to introduce the concept of spin-orbit twisted spin waves. Their group velocity acquires a nonradial component and can be controlled by the strength of the SOC. This effect opens up opportunities to control the propagation direction of spin waves by manipulating the SOC field strengths, e.g., by gating the sample. It can be exploited in spintronics to build, e.g., spin-wave routing devices or spin-wave lenses with patterning of the SOC.

F. B. and F. P. acknowledge support from the Fondation CFM, C'NANO IDF, and ANR. C. A. U. is supported by DOE Award No. DE-FG02-05ER46213. G. V. was supported by NSF Grant No. DMR-1406568. The research in Poland was partially supported by the National Science Centre (Poland) through Grants No. DEC-2012/06/A/ST3/00247 and No. DEC-2014/14/M/ST3/00484. We are thankful to L. Thevenard, C. Gourdon, and B. Jusserand for fruitful discussions.

*florent.perez@insp.upmc.fr

[1] A. V. Chumak, V. I. Vasyuchka, A. A. Serga, and B. Hillebrands, Nat. Phys. **11**, 453 (2015).
[2] Y. Kajiwara, K. Harii, S. Takahashi, J. Ohe, K. Uchida, M. Mizuguchi, H. Umezawa, H. Kawai, K. Ando, K. Takanashi, S. Maekawa, and E. Saitoh, Nature (London) **464**, 262 (2010).
[3] H. T. Nembach, J. M. Shaw, M. Weiler, E. Jue, and T. J. Silva, Nat. Phys. **11**, 825 (2015).
[4] H. Kurebayashi, J. Sinova, D. Fang, A. C. Irvine, T. D. Skinner, J. Wunderlich, V. Novák, R. P. Campion, B. L. Gallagher, E. K. Vehstedt, L. P. Zârbo, K. Výborný, A. J. Ferguson, and T. Jungwirth, Nat. Nanotechnol. **9**, 211 (2014).
[5] X. Zhang, T. Liu, M. E. Flatté, and H. X. Tang, Phys. Rev. Lett. **113**, 037202 (2014).
[6] F. Baboux, F. Perez, C. A. Ullrich, I. D'Amico, G. Karczewski, and T. Wojtowicz, Phys. Rev. B **87**, 121303 (2013).
[7] K. Zakeri, Y. Zhang, T.-H. Chuang, and J. Kirschner, Phys. Rev. Lett. **108**, 197205 (2012).
[8] F. Baboux, F. Perez, C. A. Ullrich, I. D'Amico, J. Gómez, and M. Bernard, Phys. Rev. Lett. **109**, 166401 (2012).
[9] T. Liu and G. Vignale, Phys. Rev. Lett. **106**, 247203 (2011).
[10] L. Udvardi and L. Szunyogh, Phys. Rev. Lett. **102**, 207204 (2009).
[11] A. T. Costa, R. B. Muniz, S. Lounis, A. B. Klautau, and D. L. Mills, Phys. Rev. B **82**, 014428 (2010).
[12] K. Zakeri, Y. Zhang, J. Prokop, T.-H. Chuang, N. Sakr, W. X. Tang, and J. Kirschner, Phys. Rev. Lett. **104**, 137203 (2010).
[13] K. Di, V. L. Zhang, H. S. Lim, S. C. Ng, M. H. Kuok, J. Yu, J. Yoon, X. Qiu, and H. Yang, Phys. Rev. Lett. **114**, 047201 (2015).
[14] V. E. Dmitrienko, E. N. Ovchinnikova, S. P. Collins, G. Nisbet, G. Beutier, Y. O. Kvashnin, V. V. Mazurenko, A. I. Lichtenstein, and M. I. Katsnelson, Nat. Phys. **10**, 202 (2014).
[15] J. M. Lee, C. Jang, B.-C. Min, S.-W. Lee, K.-J. Lee, and J. Chang, Nano Lett. **16**, 62 (2016).
[16] F. Baboux, F. Perez, C. A. Ullrich, G. Karczewski, and T. Wojtowicz, Phys. Rev. B **92**, 125307 (2015).
[17] J. Gaj, R. Planel, and G. Fishman, Solid State Commun. **29**, 435 (1979).
[18] See Supplemental Material at http://link.aps.org/supplemental/10.1103/PhysRevLett.000.000000, which includes Refs. [19–29], for details on sample, theory, stiffness, damping, density control and comparison with our previous model.
[19] G. Giuliani and G. Vignale, *Quantum Theory of the Electron Liquid* (Cambridge University Press, Cambridge, 2005).
[20] A. K. Rajagopal, Phys. Rev. B **17**, 2980 (1978).
[21] C. Attaccalite, S. Moroni, P. Gori-Giorgi, and G. B. Bachelet, Phys. Rev. Lett. **88**, 256601 (2002).
[22] S. De Palo, M. Botti, S. Moroni, and G. Senatore, Phys. Rev. Lett. **94**, 226405 (2005).
[23] S. A. Crooker, J. J. Baumberg, F. Flack, N. Samarth, and D. D. Awschalom, Phys. Rev. Lett. **77**, 2814 (1996).
[24] Z. Ben Cheikh, S. Cronenberger, M. Vladimirova, D. Scalbert, F. Perez, and T. Wojtowicz, Phys. Rev. B **88**, 201306 (2013).
[25] T. L. Schmidt, A. Imambekov, and L. I. Glazman, Phys. Rev. B **82**, 245104 (2010).
[26] A. Chaves, A. Penna, J. Worlock, G. Weimann, and W. Schlapp, Surf. Sci. **170**, 618 (1986).
[27] D. Richards, G. Fasol, and K. Ploog, Appl. Phys. Lett. **57**, 1099 (1990).
[28] C. Aku-Leh, F. Perez, B. Jusserand, D. Richards, W. Pacuski, P. Kossacki, M. Menant, and G. Karczewski, Phys. Rev. B **76**, 155416 (2007).
[29] B. Jussereand, F. Perez, D. R. Richards, G. Karczewski, T. Wojtowicz, C. Testelin, D. Wolverson, and J. J. Davies, Phys. Rev. Lett. **91**, 086802 (2003).
[30] F. Perez, C. Aku-leh, D. Richards, B. Jusserand, L. C. Smith, D. Wolverson, and G. Karczewski, Phys. Rev. Lett. **99**, 026403 (2007).
[31] F. Perez, Phys. Rev. B **79**, 045306 (2009).
[32] J. Gómez, F. Perez, E. M. Hankiewicz, B. Jusserand, G. Karczewski, and T. Wojtowicz, Phys. Rev. B **81**, 100403(R) (2010).
[33] F. Perez, J. Cibert, M. Vladimirova, and D. Scalbert, Phys. Rev. B **83**, 075311 (2011).
[34] $m^* = 0.105m_e$, where $m_e$ is the vacuum electron mass.
[35] E. M. Hankiewicz, G. Vignale, and Y. Tserkovnyak, Phys. Rev. B **78**, 020404 (2008).
[36] I. D'Amico and G. Vignale, Phys. Rev. B **62**, 4853 (2000).
[37] R. Winkler, *Spin-Orbit Coupling Effects in Two-Dimensional Electron and Hole Systems* (Springer, Berlin, 2003).
[38] Y. Bychkov and E. I. Rashba, J. Phys. C **17**, 6039 (1984).
[39] G. Dresselhaus, Phys. Rev. **100**, 580 (1955).
[40] A. Auerbach, *Interacting Electrons and Quantum Magnetism, Graduate Texts in Contemporary Physics* (Springer, New York, 1994).
[41] M. S. Shikakhwa, S. Turgut, and N. K. Pak, J. Phys. A **45**, 105305 (2012).
[42] B. A. Bernevig, J. Orenstein, and S. C. Zhang, Phys. Rev. Lett. **97**, 236601 (2006).
[43] A. Fresnel, Ann. Chim. Phys. **9**, 57 (1818).
[44] H. Fizeau, C. R. Acad. Sci. (Paris) **33**, 349 (1851).